



BRAIN COMMUNICATIONS

The *PSEN1* E280G mutation leads to increased amyloid- β 43 production in induced pluripotent stem cell neurons and deposition in brain tissue

Nanet Willumsen,^{1,2}  Charles Arber,¹ Christopher Lovejoy,¹ Jamie Toombs,^{1,3} Argyro Alatza,¹ Philip S. J. Weston,^{1,4} Lucia Chávez-Gutiérrez,^{5,6} John Hardy,^{1,3}  Henrik Zetterberg,^{1,3,7} Nick C Fox,^{1,4,3} Natalie S. Ryan,^{1,4,3} Tammarny Lashley^{1,2} and Selina Wray¹

Mutations in the presenilin 1 gene, *PSEN1*, which cause familial Alzheimer's disease alter the processing of amyloid precursor protein, leading to the generation of various amyloid- β peptide species. These species differ in their potential for aggregation. Mutation-specific amyloid- β peptide profiles may thereby influence pathogenicity and clinical heterogeneity. There is particular interest in comparing mutations with typical and atypical clinical presentations, such as E280G. We generated *PSEN1* E280G mutation induced pluripotent stem cells from two patients and differentiated them into cortical neurons, along with previously reported *PSEN1* M146I, *PSEN1* R278I and two control lines. We assessed both the amyloid- β peptide profiles and presenilin 1 protein maturity. We also compared amyloid- β peptide profiles in human post-mortem brain tissue from cases with matched mutations. Amyloid- β ratios significantly differed compared with controls and between different patients, implicating mutation-specific alterations in amyloid- β ratios. Amyloid- β 42:40 was increased in the M146I and both E280G lines compared with controls. Amyloid- β 42:40 was not increased in the R278I line compared with controls. The amyloid- β 43:40 ratio was increased in R278I and both E280G lines compared with controls, but not in M146I cells. Distinct amyloid- β peptide patterns were also observed in human brain tissue from individuals with these mutations, showing some similar patterns to cell line observations. Reduced presenilin 1 maturation was observed in neurons with the *PSEN1* R278I and E280G mutations, but not the M146I mutation. These results suggest that mutation location can differentially alter the presenilin 1 protein and affect its autoendoproteolysis and processivity, contributing to the pathological phenotype. Investigating differences in underlying molecular mechanisms of familial Alzheimer's disease may inform our understanding of clinical heterogeneity.

- 1 Department of Neurodegenerative Disease, UCL Queen Square Institute of Neurology, London WC1N 1PJ, UK
- 2 The Queen Square Brain Bank for Neurological Disorders, Department of Clinical and Movement Neuroscience, UCL Queen Square Institute of Neurology, London WC1N 1PJ, UK
- 3 UK Dementia Research Institute, University College London, London WC1E 6AU, UK
- 4 Dementia Research Centre, UCL Queen Square Institute of Neurology, London WC1E 6BT, UK
- 5 VIB Center for Brain and Disease Research, 3000 Leuven, Belgium
- 6 Department of Neurology, KU Leuven, 3000 Leuven, Belgium
- 7 Department of Psychiatry and Neurochemistry, Institute of Neuroscience and Physiology, Sahlgrenska Academy at University of Gothenburg, S-431 80 Mölndal, Sweden

Correspondence to: Selina Wray
Department of Neurodegenerative Disease
UCL Queen Square Institute of Neurology
London, WC1N 1PJ, UK
E-mail: selina.wray@ucl.ac.uk

Received July 23, 2021. Revised September 06, 2022. Accepted December 05, 2022. Advance access publication December 7, 2022

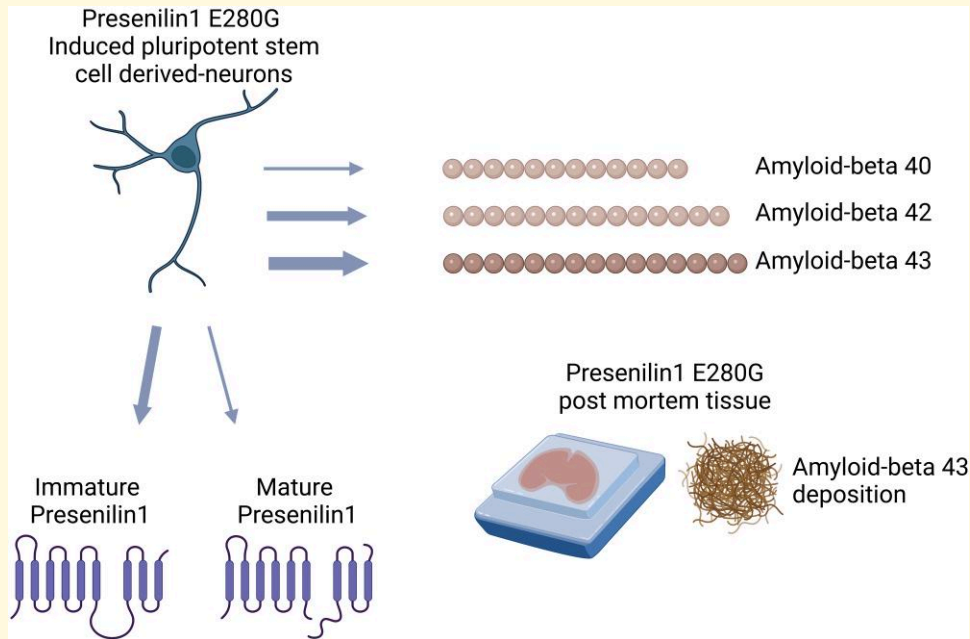
© The Author(s) 2022. Published by Oxford University Press on behalf of the Guarantors of Brain.

This is an Open Access article distributed under the terms of the Creative Commons Attribution License (<https://creativecommons.org/licenses/by/4.0/>), which permits unrestricted reuse, distribution, and reproduction in any medium, provided the original work is properly cited.

Keywords: induced pluripotent stem cells; Alzheimer's disease; γ -secretase; APP; amyloid- β

Abbreviations: A β = amyloid beta; APP = amyloid precursor protein; CAA = cerebral amyloid angiopathy; CWP = cotton wool plaque; DAP = 4',6-diamidino-2-phenylindole; FAD = familial Alzheimer's disease; ICC = immunocytochemistry; IHC = immunohistochemistry; iPSCs = induced pluripotent stem cells; NTF = N-terminal fragment; PSEN1 = Presenilin 1; RIPA = radio immunoprecipitation assay buffer; SNP = single nucleotide polymorphism; WT = wild type

Graphical Abstract



Introduction

Alzheimer's disease is defined by the cerebral accumulation of pathological misfolded proteins into amyloid beta (A β) plaques and neurofibrillary tangles containing tau.¹⁻³ Familial Alzheimer's disease (FAD) shares these pathological features with sporadic Alzheimer's disease (sAD). However, FAD is caused by rare autosomal dominant mutations in the presenilin 1 (*PSEN1*), *PSEN2* or amyloid precursor protein (*APP*) genes and *APP* duplications.⁴⁻⁹

The presenilin 1 protein (*PSEN1*) is the catalytic component of the γ -secretase complex, responsible for the cleavage of APP.^{10,11} In the amyloidogenic pathway, APP is cleaved by β -secretase (*BACE1*) releasing the sAPP β fragment.¹² The remaining membrane-bound C99 fragment undergoes an initial epsilon cleavage, releasing an APP intracellular C domain and a membrane-bound A β peptide. Sequential carboxypeptidase-like cleavages of A β by the γ -secretase complex releases A β peptides of varying length.¹³ Epsilon A β cleavage occurs at residue 48 or 49, giving rise to two cleavage pathways of decreasing peptide length (A β 49 > 46 > 43 > 40 and A β 48 > 45 > 42 > 38).¹⁴ In *PSEN1*-FAD, there is a loss of processivity leading to qualitative shifts towards longer A β peptides.¹⁵

Recently, there have been multiple papers that have generated induced pluripotent stem cells (iPSCs) from FAD and Down's syndrome patient fibroblasts, reviewed in.¹⁶ Studies

have revealed that specific FAD mutations produce very distinct A β ratios, as shown in both iPSC differentiated into neurons¹⁷ and in other cell-based and activity assay models,¹⁸⁻²⁰ recapitulating aspects of disease *in vitro*. Importantly, these A β ratios are likely to reflect early perturbations in A β processing, revealing early disease mechanisms.

Compared with wild-type (WT) *PSEN1*, most pathogenic *PSEN1* mutations cause an increase in the ratio of A β 42 to total A β , and notably an increased A β 42:40 ratio.²¹ However, the mechanism by which ratios are altered differs by mutation. Specific *PSEN1* mutations affecting γ -secretase activity can influence both absolute amounts of A β and the A β cleavage pathway selection, leading to altered ratios of the peptides within those pathways.²²

Pathogenic *PSEN1* mutations appear to consistently hinder sequential carboxypeptidase cleavage, leading to the release of longer A β peptides, alterations of which can be measured via the A β 42:38 and A β 43:40 ratios. This results in a relative increase in, and release of, longer A β peptides which are more prone to aggregation,^{6,15,22} in turn leading to more oligomeric A β and greater extracellular deposition.²³ Mutations that severely compromise γ -secretase carboxypeptidase activity affect residues that map near the proposed γ -secretase active site.^{20,24}

Upon γ -secretase complex assembly full-length *PSEN1* undergoes autoendoproteolysis to produce cleaved *PSEN1*,

consisting of the *PSEN1* N-terminal fragment (NTF) and C-terminal fragment.²⁵ Mutations near the endoproteolytic site are proposed to inhibit endoproteolysis,²⁶ which can lead to altered processivity.²⁷ Interestingly, even within the γ -secretase complex bearing full-length *PSEN1*, the catalytic pore is still able to be formed,²⁸ which suggests that proteolytic activity can still occur, although it may be reduced.

In some mutations, an increase in the ratio of A β 43 compared with other peptide lengths or increased absolute levels has been linked to an increase in the full-length form of *PSEN1*. The *PSEN1* R278I mutation has previously been shown to have increased full-length *PSEN1* and A β 43 ratio in patient iPSC-derived neuronal lines by our group.¹⁷ Increased A β 43 and full-length *PSEN1*, with reduced A β 40, was also observed in the R278I mutation mouse embryonic fibroblast CF-1 (MEF) cell line^{19,29,30} and mouse models.³⁰ Importantly, alterations in *PSEN1* maturity were not caused by differences in *PSEN1* expression, and *APP* expression was not altered,¹⁷ implying specific mutations affect disease via influencing *PSEN1* structure/function. Along with R278I, other mutations associated with high A β 43 are located around the intracellular loop. Another important mutation located in this area is the E280G mutation. Clinically, the E280G mutation is associated with atypical clinical presentations, including spastic paraparesis and marked white matter hyperintensities on MRI.^{31,32} Pathologically, a brain biopsy from a *PSEN1* E280G carrier showed numerous large non-cored A β deposits as cotton wool plaques (CWPs) and severe cerebral amyloid angiopathy (CAA).³¹ An individual with the *PSEN1* E280Q mutation has also had a similar CWP pathology observed post-mortem.³³ HEK lines expressing the E280G mutation show significantly increased A β 42 concentration, non-significantly increased A β 40 concentration and an overall significantly increased A β 42:40 ratio in conditioned media compared with controls.³⁴ However, as discussed by the authors, these results suffer from the caveat that only mutated *PSEN1* is expressed in these lines compared with heterozygous mutation carriers where WT *PSEN1* is also expressed. In another study, cloned γ -secretase with a range of *PSEN1* mutations was purified, WT or mutant γ -secretase was mixed with APP-C99 in a detergent-based assay and incubated at 37°C for 16 h. A β peptides produced in the detergent-based assay were measured using an AlphaLISA assay. The assays revealed greater amounts of A β 42 compared with A β 40 and a higher A β 42:40 ratio in association

with the *PSEN1* E280G mutation, while western blot images also suggested the presence of full-length *PSEN1*, possibly due to reduced endoproteolytic processing.²⁰ A β 43 has not, however, been assessed in the *PSEN1* E280G mutation.

In this study, we generated E280G iPSCs from two clinically affected FAD patient donors. We went on to investigate A β profiles using ratios measured via an enzyme-linked immune-sorbent assay (ELISA) and an electrochemiluminescence assay, and *PSEN1* protein maturation in iPSC-derived neurons, with the hypothesis that the E280G mutation decreases *PSEN1* autoendoproteolysis, resulting in the enhanced generation of A β 43, similar to the proximal *PSEN1* R278I mutation. Finally, we compared these findings to post-mortem tissue from E280G carriers.

Materials and methods

Cell culture

Cell lines used in this study are summarized in Table 1. The study was approved by the joint research ethics committee of the National Hospital for Neurology and Neurosurgery and the Institute of Neurology (09/H0716/64), and informed consent was gained for all samples. All reagents were purchased from Thermo Fisher Scientific unless specified. Fibroblasts were cultured as previously described.³⁵ Fibroblasts underwent episomal reprogramming according to Okita *et al.*³⁶ Fibroblasts underwent nucleofection with episomal DNA coding for OCT4 and shRNA against p53, KLF4, SOX2 and c-MYC using plasmids #27077, #27078, and #27080 which were obtained from Addgene. Nucleofection was performed using the Lonza P2 Nucleofection kit (Amaxa PBP2-00675) as per manufacturer's instructions.

After nucleofection, cells were grown on geltrex (1:100, DMEM/F12) (A1413302, Life Technologies), maintained in fibroblast media which was changed every three days.

Six days after electroporation, cells were lifted with 1 × trypsin (15090-046, Gibco) and resuspended in fibroblast media on cultured on geltrex-coated MEF feeder layer coated (ATCC® SCRC-1040TM) 10 cm dishes (172958, Nunc). On Day 8 after nucleofection, media was switched to human embryonic stem cell media (DMEM/F12 Glutamax, 20% Knock out Serum, 2 mM L-glutamine, 1 × Non-essential amino acids, 50 U/ml pen & 50 µg/ml strep, all from Gibco, 50 µM 2-Mercaptoethanol (ThermoFisher),

Table 1 Cell lines used in this study

Line name	Mutation	Sex	age at onset	Age at biopsy	APOE genotype	Origin
CTL1 (SIGi001-A-1)	—	F	—	24	3/4	Sigma Aldrich/EBiSC
CTL2 (RBi001-A)	—	M	—	45–49	3/3	Sigma Aldrich/EBiSC
M1461	<i>PSEN1</i> M146I	M	Presymptomatic	38	3/3	StemBancc
R278I	<i>PSEN1</i> R278I	M	58	60	2/4	Arber <i>et al.</i> 2019
E280G.A	<i>PSEN1</i> E280G	M	41	45	3/3	Generated in this study
E280G.B	<i>PSEN1</i> E280G	M	38	49	3/4	Generated in this study

20 ng/ml Fibroblast Growth Factor-basic (Peprotech)) and changed daily. Nascent iPSC colonies were picked and transferred into feeder-free conditions (Essential eight media and geltrex matrix). iPSCs were passaged using 0.5 mM ethylenediaminetetraacetic acid.

iPSCs were differentiated into cortical neurons according to the Shi *et al.*³⁷ protocol. Briefly, iPSCs were grown to 100% confluence, and the media was changed to neural induction media [N2B27 containing 10 μ M SB431542 (Tocris) and 1 μ M dorsomorphin (Tocris)]. N2B27 media consists of a 1:1 mixture of Dulbecco's modified eagle medium F12 (DMEM-F12) and Neurobasal supplemented with 0.5X N2, 0.5X B27, 0.5X non-essential amino acids, 1 mM L-glutamine, 25 U/ml pen & 25 μ g/ml strep, 50 μ M β -mercaptoethanol and 2.5 μ g/ml insulin. At Day 12, the precursors were passaged by using a cell scraper (541070, Greiner Bio-One International) onto laminin-coated wells and at Day 18 passaged using dispase and plated in laminin-coated wells (Sigma) in N2B27 media. The final passage was performed at Day 35 using accutase and maintained in N2B27 media on poly-L-ornithine (Sigma) and laminin (Sigma) coated wells in N2B27 media until the required time point. Neurons were analysed at 100 days post-neural induction. One hundred days were selected as it represents the end of corticogenesis and detectable levels of secreted A β .³⁸

Karyotyping

DNA was harvested using the TRIzol™ (15596026, Invitrogen) protocol according to manufacturer's instructions. Briefly, cells were homogenized in 1 ml TRIzol™ followed by the addition of 200 μ l Chloroform (22711.290, VWR), shaken vigorously and then incubated for 3 mins followed by centrifugation at 12 000g_(av), 4°C for 15 mins. After isolating and removing the aqueous phase, the DNA-containing interphase was removed from the organic phase by adding 300 μ l of 100% ethanol was added and samples were shaken, incubated for 3 mins and centrifuged at 2000 g_(av), 4°C for 5 mins. The DNA was washed twice by the addition of 0.1 M trisodium citrate in 10% ethanol, pH 8.5 followed by incubation for 30 mins with regular inversion followed by centrifugation at 2000g_(av), 4°C for 5 mins. The pellet was resuspended in 1.5 ml 75% ethanol and incubated for 20 mins with regular inversion followed by centrifugation at 2000 g_(av), 4°C for 5 mins. The pellet was air dried for 10 mins before resuspension in 300 μ l 8 mM NaOH, followed by centrifugation at 12 000g_(av), 4°C for 10 mins. Genomic DNA from the two patient PSEN1 E280G lines, named E280G.A and E280G.B, were analysed for chromosomal abnormalities using the hPSC Genetic Analysis Kit (Stem Cell Technologies) and the StemCell genetic analysis app. Amplification in a minimal critical region of chromosome 17 of the E280G.A line was observed, with a calculated copy number of 2.44. There were no significant amplifications in the E280G.B line. Additional chromosomal sites (Chr 1q, Chr 4p, Chr 8q,

Chr 10p, Chr 12p, Chr 18q and Chr Xp) showed no significant abnormalities.

NanoString Stem Cell Characterization Panel

RNA was harvested from iPSCs 2 days after passage via Monarch total RNA miniprep kit (NEB). 100 ng was used for Nanostring analysis on the nCounter Stem Cell Characterization Panel. The expression of 770 genes was analysed on the nSolver software to compare grouped control (CTL1 and CTL2) and grouped E280G (E280G.A and E280G.B) data. Linear regression analysis was performed using GraphPad Prism.

Immunocytochemistry

Coverslips were washed with Dulbecco's phosphate-buffered saline (PBS) and fixed for 15–20 min in 4% formaldehyde followed by excess 1X PBS wash and stored in PBS at 4°C. Coverslips were blocked in 5% BSA/0.3% PBS-triton-X-100 followed by primary antibody incubation (Table 2) in block solution for 2 hrs or 4°C overnight. After three washes in 1X PBS-0.3% triton, a secondary antibody (Table 2) in block solution was added for 1 h, in the dark. Following a PBS-0.3% triton wash, DAPI (1:5000, D1306, Invitrogen) was added as a nuclear counterstain and incubated in the dark. Cells were washed once with PBS-triton followed by 1X PBS, mounted onto slides with fluorescence mounting medium (S3023, DAKO) and imaged on a Leica DM5500 B microscope using Leica Application suite X software (Leica microsystems, Wetzlar, Germany).

Conditioned cell media collection

Cortical neurons were incubated in N2B27 media for 48 h prior to collection, as described previously.¹⁷ Conditioned media was centrifuged at 2000 g_(av) for 5 min at RT, with 1 ml aliquoted in Sarstedt 2 mL PP tubes (72.694.406) and stored at –80°C.

Western blotting

Cells that had been used for conditioned media collection were lysed in radioimmunoprecipitation assay buffer (RIPA) containing phosphatase and protease inhibitors (Roche). Using the Bio-Rad DC™ Protein Assay, 5 μ l of sample and standards (1:1 dilutions of Bovine Serum Albumin in RIPA from 4 mg/ml to 0.125 mg/ml + a RIPA blank) was added to reagent A + S, followed by reagent B, in triplicate. After plate shaking and 15 min development time, absorbance was measured at 750 nm on a Spark™ 10 m plate reader (Tecan). Concentration was calculated from the standard curve using the equation $x = (y - m)/b$. Lysates of 30 μ g loaded with NuPage™ LDS sample buffer and NuPAGE™ reducing agent were denatured at 70°C for 10 min followed by brief centrifugation. Electrophoresis was conducted on a NuPage™ 10% Bis-Tris gel in MES

Table 2 Antibodies used in this study

Antibody	Company	Species	Dilution	Purpose
SSEA4	Biologend MC-813–70	Mouse	1:300	ICC
OCT4	Santa Cruz SC-8628	Rabbit	1:400	ICC
NANOG	Cell Signaling Technology D73G4	Rabbit	1:500	ICC
FOXG1	Abcam Ab18259	Rabbit	1:500	ICC
PAX6	DSHB	Mouse	1:5	ICC
TBR1	Abcam AB31940	Rabbit	1:300	ICC
TUJ1	Biologend 801201	Mouse	1:1000	ICC
TUJ1	Biologend 802001	Rabbit	1:1000	ICC
488 Donkey anti-Rabbit	Alexa Fluor® A21206		1:5000	ICC
594 Donkey anti-Mouse	Alexa Fluor® A21203		1:5000	ICC
488 Donkey anti-mouse	Alexa Fluor® A-21202		1:5000	ICC
594 Donkey anti-Rabbit	Alexa Fluor® A21207		1:5000	ICC
PSEN1 N-term	Millipore MAB1563	Rat	1:500	Western blot
β -Actin	Sigma	Mouse	1:1000	Western blot
Goat anti-rat	Alexa Fluor® A21096		1:10,000	Western blot
Goat anti-mouse	Li-cor 926-68071		1:10 000	Western blot
A β 40	Merk AB5074P	Rabbit	1:100	IHC
A β 42	BioLegend 805509	Mouse	1:500	IHC
A β 43	BioLegend 805607	Mouse	1:500	IHC
Swine anti-rabbit	DAKO E0353		1:200	IHC
Rabbit anti-mouse	DAKO E0354		1:200	IHC

SDS running buffer at 150 V for 1 h 30 mins. Transfer to nitrocellulose membrane was conducted at 30 V for 1 h. The membrane was blocked in 5% BSA/0.1% PBS-tween20 (PBS-T) and incubated in anti-PSEN1 overnight at 4°C. The membrane was washed three times with 0.1% PBS-T and incubated in a secondary antibody (Table 2) for 1 h, in the dark. The membrane was washed once with 0.1% PBS-T and twice with PBS before imaging on an Odyssey Fc (Li-cor). The membrane was then incubated for 1 h in anti- β -actin, washed three times with 0.1% PBS-T and incubated in a secondary antibody (Table 2) for 1 h, in the dark. The membrane was washed once with 0.1% PBS-T and twice with PBS before imaging on an Odyssey Fc (Li-cor). Data from the two control lines (CTL1 and CTL2) were pooled and comparisons were made between all cell lines.

Immunoassays

Solid phase sandwich, ELISA for A β 1-43 (27710, IBL) was conducted using D100 neuron-conditioned cell media according to manufacturer's instructions. Briefly, 100 μ l of calibrator, control and samples were added in duplicate to individual wells coated with an A β 1-43 peptide-specific capture antibody. A labelled detection antibody (82E1) was applied followed by chromogen incubation and the eventual addition of the stop solution. The plate was then read at 450 nm, with a reference of 650 nm (FLUOstar Omega Microplate Reader, BMG Labtech). A β 38/40/42 in D100 neuron-conditioned cell media were measured by electrochemiluminescence using the V-PLEX A β Peptide Panel 1 (6E10) Kit (1 Plate) (K15200E, Mesoscale Discovery), according to manufacturer's instructions. Briefly, samples

were diluted 1:1 in diluent 35 and added in duplicate to individual wells which were coated in mouse monoclonal peptide-specific capture antibodies for human A β x-38/x-40/x-42. Samples were incubated with anti-A β antibody (6E10 clone) as the detection antibody conjugated with an electrically excitable SULFO-TAG. Measurements were made using the MESO QuickPlex SQ 120, MSD. Concentrations were calculated from the ECL signal using a four-parameter logistic curve-fitting method with the MSD Workbench software package. Absolute levels of secreted A β 43, A β 42, A β 40, and A β 38 were measured and converted to ratios for comparison. Data from the two control lines (CTL1 and CTL2) were pooled and comparisons were made between all cell lines, except for the E280G.B line in A β 38 analyses due to the low number of inductions ($n = 2$).

Complementary DNA synthesis and quantitative PCR (qPCR)

RNA was harvested using the TRIzol™ (15596026, Invitrogen) protocol and stored at -80° C. Complementary DNA was generated from 500 ng of harvested RNA using the SuperScript IV Reverse Transcription Kit (18091050, ThermoFisher) and random hexamers following the manufacturer's instructions. qPCR for each induction (run in triplicate) was performed using Power SYBR™ Green (ThermoFisher) on the Mx3000P qPCR system (Agilent). The following primers were used: T-box Brain Transcription Factor 1 (TBR1, F: AGCAGCAAGATCAAAAAGTGAGC R: ATCCA CAGACCCCTCACTAG), Special AT-rich sequence-binding protein 2 (SATB2, F: CAACGCAACTAATAATCATCTCCC R: GAGAAAGGGCTGAGAACCCG), Class III beta-tubulin

(T_{UJ1}, F: CATGGACAGTGTCCGCTCAG R: CAGGCA GTCGCAGTTTTTCAC) and PSEN1 (F: CAATACTGTACG TAGCCAGA R: AATGGGGTATAGATTAGCTG). Data were normalized to housekeeping gene *RPL18a* (F: CCCA CAACATGTACCGGGAA R: TCTTGGAGTCGTGGAAC TGC).

Immunohistochemistry

All three FAD cases assessed in this study were obtained through the brain donation programme of the Queen Square Brain Bank for Neurological Disorders, Department of Clinical and Movement Neurosciences, UCL Queen Square Institute of Neurology. The protocols used for brain donation and ethical approval for this study were approved by a London Research Ethics Committee and tissue is stored for research under a license from the Human Tissue Authority. The standard diagnostic criteria for the neuropathological diagnosis of Alzheimer's disease were used in all cases.^{1-3,39} For a summary of cases, see Table 3. Paraffin-embedded serial sections of 8 µm thickness from the temporal cortex were cut. Serial sections were used for Aβ immunohistochemistry (IHC). Slides were pre-treated in formic acid followed by a pressure cooker in citrate buffer pH 6.0. Endogenous peroxidase activity was blocked with 0.3% H₂O₂ in methanol and non-specific binding with 10% dried milk solution. Sections were incubated with the primary antibodies (Table 2) overnight at 40°C, followed by biotinylated secondary antibody ABC complex (30 minutes; PK-6100, Vector Laboratories Ltd). Colour was developed with di-aminobenzidine/H₂O₂. Micrographs were taken on a brightfield microscope and images analysed for percentage area staining using Halo software (Indica Labs) with the Indica Labs standard macro (Area Quantification v1) optimized for each Aβ antibody.

Statistical analysis

Cell data were checked for normality using QQ plots. For statistical analysis, the CTL1 and CTL2 lines have been pooled. When needed for western blot and qPCR analysis, CTL2 was used for normalization. Cell data were assessed using one-way ANOVA with a probability value of less than $P < 0.05$ considered significant. When ANOVA analysis reached statistical significance, Tukey's *post hoc* test was used, adjusting the significant level appropriately for the analysis conducted. All cell data statistics were conducted on GraphPad Prism.

Results

Generation and characterization of iPSCs from two PSEN1 E280G mutation carriers

Fibroblasts from two *PSEN1* E280G mutation carriers were reprogrammed to iPSCs via episomal reprogramming. Confirmation of successful reprogramming in the newly generated *PSEN1* E280G lines was confirmed by immunocytochemistry (ICC) which showed that all iPSC lines expressed the markers of pluripotency NANOG and SSEA4 (Fig. 1A). Chromosomal analysis indicated stable karyotypes with the exception of a potential amplification in a minimal critical region of chromosome 17 in the *PSEN1* E280G.A line, with a calculated average copy number of 2.44 (Fig. 1B). The exact primer probe binding sequence is not disclosed by the StemCell technologies thus the exact region of amplification cannot be confirmed. Amplifications in 17q are commonly found in hPSC cultures indicating a pro-survival benefit to stem cells.⁴⁰ Expression of 770 stem cell-associated genes was analysed on the NanoString Stem Cell Characterization Panel. Analysis of grouped data to compare control lines (CTL1 and CTL2) with E280G lines (E280G.A and E280G.B) displayed a high correlation ($R^2 = 0.9932$), representing a similar stem cell expression profile in the newly derived lines compared with established iPSCs (Supplementary Fig. 1). Sanger sequencing of genomic DNA obtained from iPSCs confirmed the presence of the E280G mutation within both cell lines (Fig. 1C).

Differentiation of E280G iPSC into cortical neurons

Together with two control lines, and two previously characterized FAD iPSC lines (*PSEN1* M146I and R278I),¹⁷ the newly generated lines were subjected to cortical differentiation to generate the cell type affected in FAD. ICC was conducted on all control and FAD cell lines to investigate forebrain patterning at Day 25 via Forkhead Box G1 (FOXG1) and Paired box protein Pax-6 (PAX6) staining (Fig. 2A), as well as a neuronal phenotype at Day 100 with neuron-specific TUJ1 and lower cortical layer neuron marker TBR1 (Fig. 2B),

RNA from cell lines underwent qPCR analysis to assess the phenotype. Expression was normalized to housekeeping gene *RPL18a* prior to comparison. Expression of TBR1

Table 3 Summary of post-mortem brain tissue used in this study

Mutation	APOE genotype	Sex	Age at onset	Disease duration (years)	Braak Tau	Thal Phase	CERAD	PM delay (hrs/mins)
<i>PSEN1</i> M146I	23	M	48	6	>6	5	Frequent	115:35:00
<i>PSEN1</i> R278I	23	M	54	12	6	5	Frequent	77:45:00
<i>PSEN1</i> E280G	34	F	42	11	6	5	Frequent	11:00

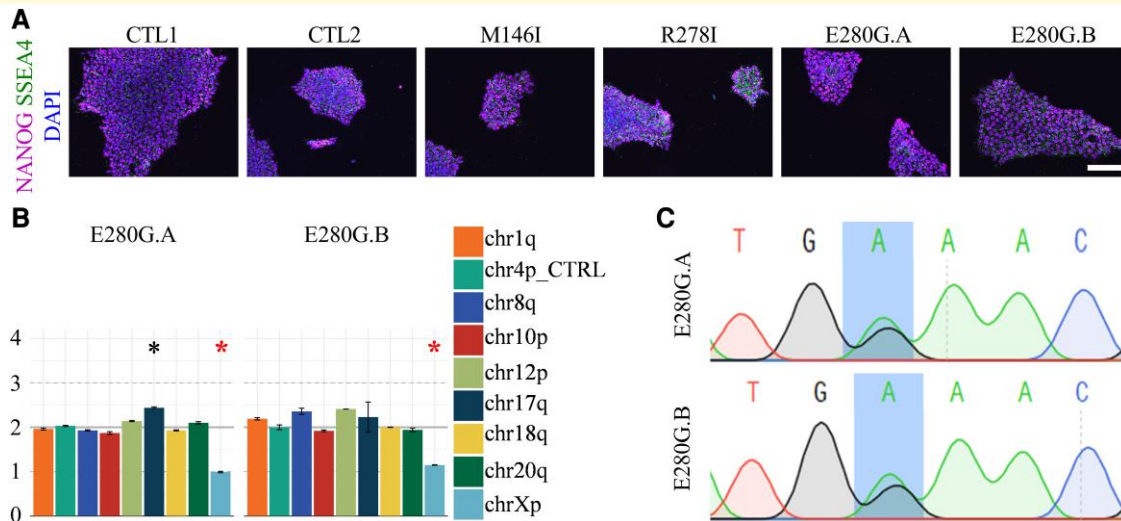


Figure 1 iPSC generation and characterization of new E280G lines. **(A)** Representative images of iPSC lines show expression of endogenous pluripotency markers in all lines. NANOG, magenta; SSEA4, green; DAPI, blue. Scale bar represents 100 μ m. **(B)** Karyotype stability analysis via genomic PCR. Compared with controls, a significant amplification indicated (green asterisk *) for primer pair chr17q in the E280G.A line and the red asterisk indicates significant difference for chrXp primer pair, confirming male sex of samples. **(C)** Sequencing reads in *PSEN1* exon 8 confirm E280G SNP (A > G) in one allele, confirming heterozygous mutation in both cell lines.

(Fig. 2C, lower layer cortical neurons) was compared across cell lines, relative to the CTL2 line. There was a significant difference across cell lines ($P=0.02$, one-way ANOVA) with a significant difference between the control and E280G.B lines ($P=0.02$, Tukey's multiple comparison test). There was no significant difference in SATB2 expression (Fig. 2D, upper layer neurons) or in TUJ1 (Fig. 2E, pan-neuronal marker) expression.

Mutation-specific effects on A β species generation

To explore A β processing down the A β 48/49 pathways *in vitro* (Fig. 3A), we assessed A β peptide production in the control lines (pooled data), and the four FAD patient-derived lines (*PSEN1* M146I, *PSEN1* R278I and two *PSEN1* E280G). There was a significant difference in the A β 42:40 ratio, indicative of both γ -secretase epsilon cleavage efficiency and selection of the A β 48 or 49 pathway, across the cell lines ($P < 0.0001$). Compared with controls, there was a significantly increased ratio in the M146I, E280G.A and E280G.B lines ($P < 0.0001$, $P < 0.0001$, $P = 0.006$). M146I and E280G.A also had significantly increased A β 42:40 ratios compared with R278I ($P = 0.0003$, $P = 0.003$). The M146I line also had a significantly increased A β 42:40 ratio compared with E280G.B ($P = 0.01$), Fig. 3B.

The A β 43:40 ratio, indicative of γ -secretase carboxypeptidase cleavage efficiency in the A β 49 pathway, was significantly different between cell lines ($P < 0.0001$). Compared with controls, there was a significantly higher A β 43:40 ratio in the R278I, E280G.A and E280G.B lines ($P = 0.0001$, $P < 0.0001$, $P = 0.002$). The A β 43:40 ratio in the R278I, E280G.A and E280G.B lines was also significantly higher

compared with M146I ($P = 0.0004$, $P = 0.0002$, $P = 0.004$), Fig. 3C.

The ratio of A β 42:38, indicative of γ -secretase carboxypeptidase cleavage efficiency in the A β 48 pathway, was compared across all lines, excluding E280G.B due to low n number ($n = 2$). The ratio was significantly different across the cell lines ($P < 0.0001$, ANOVA). Compared with controls, M146I, R278I and E280G.A had a significantly increased A β 42:38 ratio (both $P < 0.0001$, Tukey's test). The M146I line had a significantly increased ratio compared with R278I, and significantly reduced ratio compared with E280G.A (Both $P < 0.0001$). The R278I line had a significantly reduced ratio compared with E280G.A ($P < 0.0001$), Fig. 3D.

There was a significant difference across the lines (excluding E280G.B) in the ratio of A β 38:40 ($P < 0.0001$), which indicates γ -secretase epsilon cleavage efficiency in the A β 48:49 pathways. Controls had a significantly increased A β 38:40 ratio compared with R278I and E280G.A lines ($P = 0.008$, $P < 0.0001$). The M146I line had a significantly increased A β 38:40 ratio compared with E280G.A ($P = 0.0002$). R278I also had a significantly increased A β 38:40 ratio compared with E280G.A ($P = 0.02$), Fig. 3E.

Pathway 43, also indicative of γ -secretase epsilon cleavage to the A β 48 or 49 pathway, significantly differed across cell lines ($P = 0.002$). Compared with controls, there was a significantly decreased A β 42:43 ratio in the R278I, E280G.A and E280G.B lines ($P = 0.04$, $P = 0.05$, $P = 0.05$). Additionally, compared with M146I, there was a significantly decreased A β 42:43 ratio in the R278I, E280G.A and E280G.B lines ($P = 0.01$, $P = 0.01$, $P = 0.01$), Fig. 3F.

These data support *PSEN1* mutation-specific effects on APP processing and A β species generation. Specifically, the

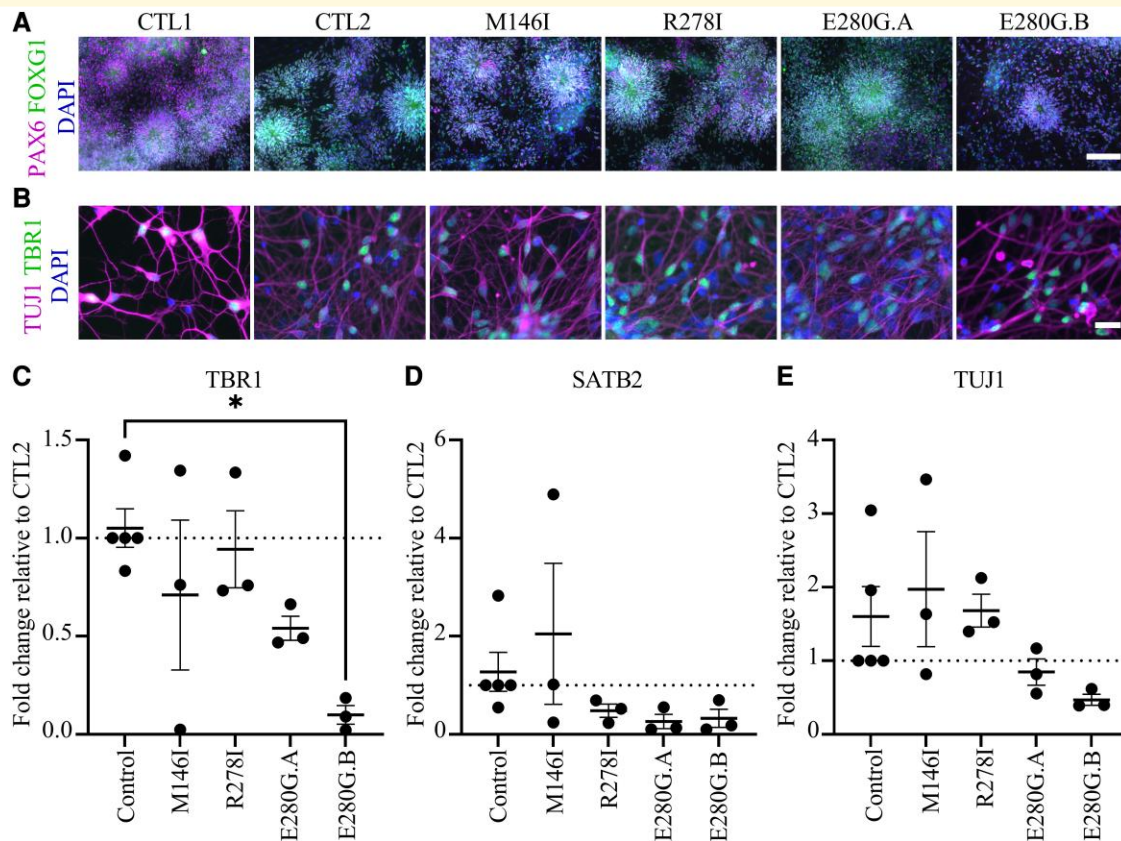


Figure 2 Characterization of iPSC-cortical neurons. Control, M146I, R278I and E280G iPSC lines were differentiated into cortical neurons. **(A)** Confirmation of cortical neurogenesis in D25 cortical neurons. Representative images shown. DAPI, blue; PAX6, magenta; FOXG1, green. White scale bar represents 100 μ m. **(B)** Confirmation of neuronal phenotype in D50 cortical neurons. DAPI, blue; neuronal tubulin (TUJ1), magenta; deep layer cortical neuronal marker TBR1, green. White scale bar represents 20 μ m. **(C)** TBR1 expression measured by qPCR significantly differed across cell lines. **(D)** SATB2 expression measured by qPCR did not significantly differ across cell lines. **(E)** TUJ1 expression measured by qPCR did not significantly differ across cell lines. $n = 3$ inductions per cell line with each individual dot representing qPCR data from triplicate technical repeats, except in the CTL1 line where $n = 2$ inductions. Error bars represent mean and SEM. One-way ANOVA with Tukey's multiple comparison, * $P < 0.05$

data from E280G support a relative increase in the generation of A β 42 as well as a relative increase in A β 43, explained by reduced processivity in both tripeptide cleavage pathways (48> and 49>).

PSEN1 autoendoproteolysis is affected by the E280G mutation

PSEN1 mutations have been shown to alter γ -secretase stability.^{38,41} By using western blots to probe for the PSEN1-NTF, the presence of cleaved and full-length PSEN1 was assessed in the neurons, Fig. 4A.

Firstly, the amount of full-length PSEN1 (46 kDa), relative to actin, was normalized to CTL2. Protein expression was then compared between the control lines (pooled data), and the four FAD patient-derived lines (*PSEN1* M146I, *PSEN1* R278I and two *PSEN1* E280G). Full-length PSEN1 levels statistically differed across lines ($P = 0.04$), with significantly increased levels in the R278I

line compared with the control group ($P = 0.03$), with a notable trend for increased levels in the E280G lines, see Fig. 4B.

Secondly, the amount of PSEN1-NTF (25 kDa), relative to actin and normalized to CTL2, was then compared between the control lines (pooled data), and the four FAD patient-derived lines. PSEN1-NTF levels indicate effective autocleavage of PSEN1 into the N and C-terminal fragments. PSEN1-NTF significantly differed across lines ($P = 0.0007$). Compared with the control group, PSEN1-NTF was significantly higher in the E280G.A and E280G.B lines ($P = 0.02$ and $P = 0.006$, respectively) and significantly higher in the E280G.A and E280G.B lines compared with the R278I lines ($P = 0.005$ and $P = 0.002$, respectively), see Fig. 4C.

Finally, the levels of full-length PSEN1 relative to PSEN1-NTF, normalized to the CTL2 line was compared between the control lines (pooled data), and the four FAD patient-derived lines. This ratio was significantly different across lines ($P < 0.0002$) with higher full-length PSEN1 levels in the R278I line compared with the control group ($P < 0.0001$),

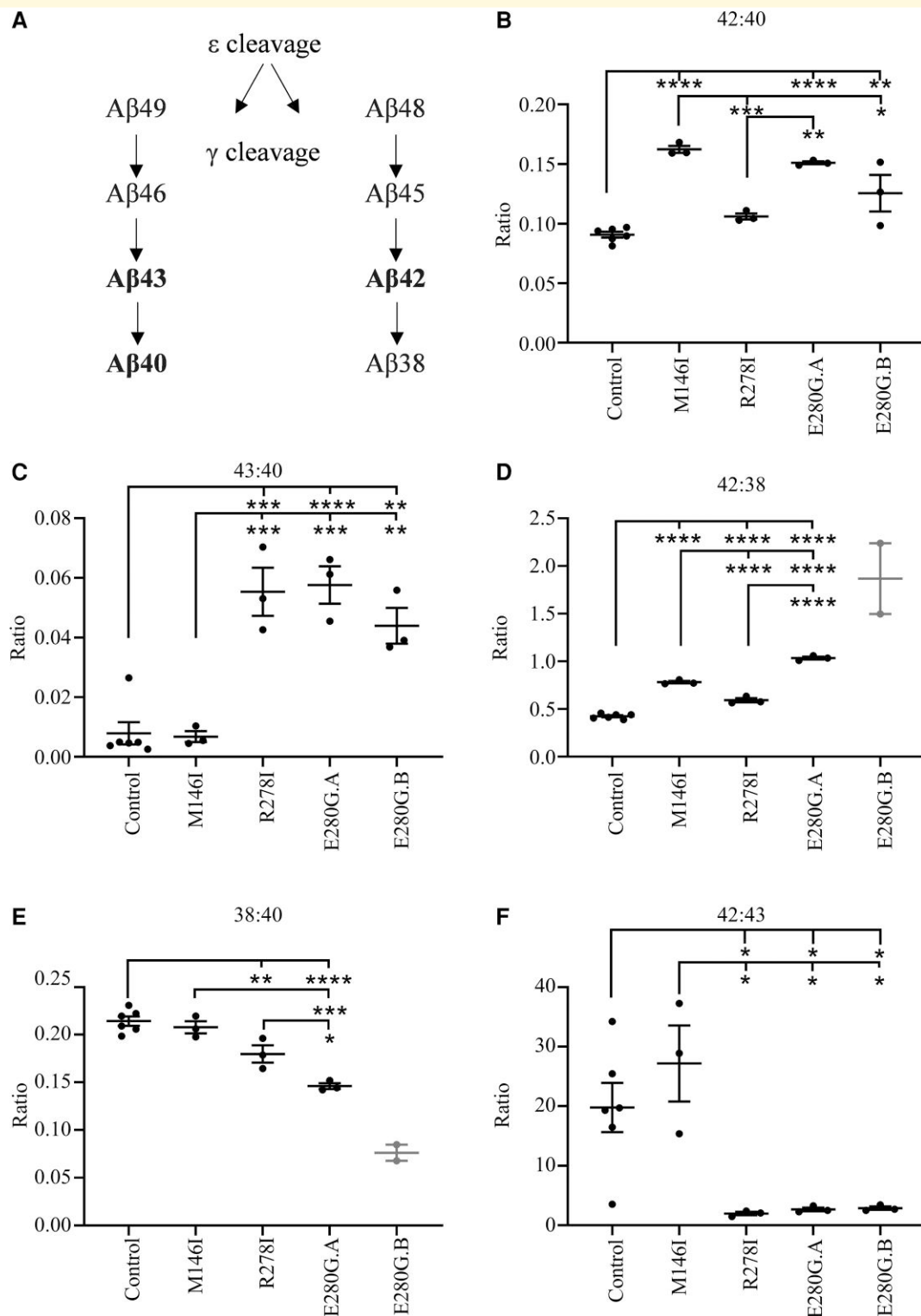


Figure 3 Characterization of the A β profile of iPSC-derived neurons. (A) A β cleavage down the A β 48 or A β 49 pathways. (B) A β 42:40 used as a FAD biomarker. (C) A β 43:40 used as a FAD biomarker. (D) A β 42:38 as a measure of processivity. (E) A β 38:40 as a comparison of carboxypeptidase activity in the two cleavage pathways. (F) A β 42:43 representing endopeptidase activity and tripeptide cleavage path choice. Each data point represents the mean value of duplicate technical repeats from a single induction. Control lines $n = 6$ (mean from 3 individual inductions from both control I + 2), *PSEN1* mutation lines $n = 3$ (mean from three individual inductions), except for E280G.B A β 38 data points, where $n = 2$ as A β 38 levels were below detection limits on the V-PLEX A β Peptide Panel I (6E10) Kit for I and thus have been excluded from comparisons involving A β 38; however data points are still displayed for observation. Error bars represent mean and standard error of the mean (SEM), one-way ANOVA with Tukey's test, * $P < 0.05$, ** $P < 0.01$, *** $P < 0.001$, **** $P < 0.0001$

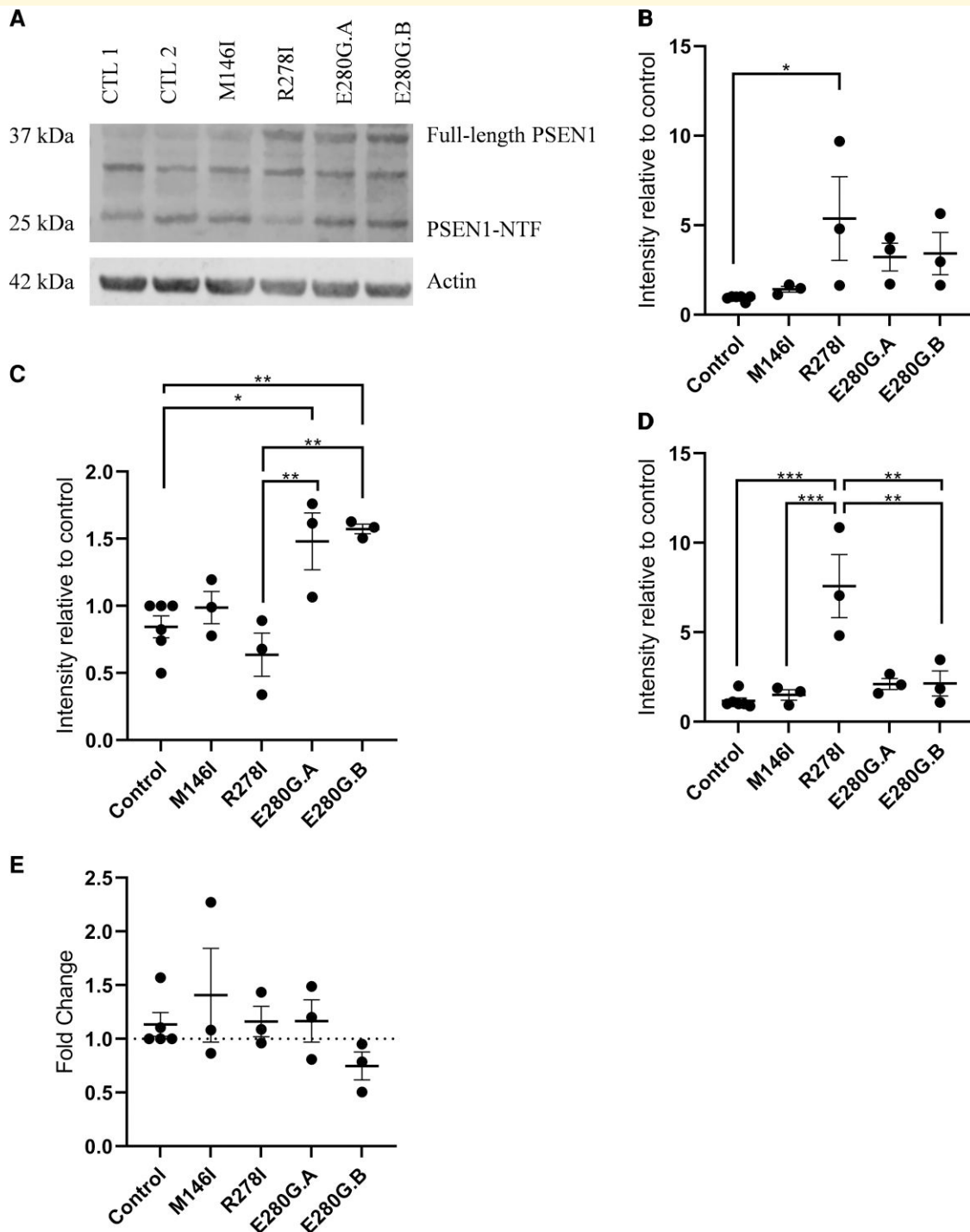


Figure 4 *PSEN1* peptide autoproteolysis and maturity in neurons. **(A)** Representative western blot suggesting increased full-length *PSEN1* in R278I and E280G lines and decreased *PSEN1*-NTF in the R278I line. An unidentified unspecific band is present at 33–34 kDa. **(B)** Full-length *PSEN1* was significantly higher in the R278I line compared with control. **(C)** *PSEN1*-NTF was significantly higher in the E280G lines compared with the control, M146I and R278I lines. **(D)** Full-length *PSEN1* relative to *PSEN1*-NTF was significantly higher in the R278I line compared with control, M146I and E280G lines. Each datapoint (4B–D) represents relative band intensity (normalized to CTL2) from a single induction. **(E)** No significant difference in *PSEN1* expression across cell lines, each datapoint represents normalized expression from a single induction, run in triplicate. One-way ANOVA with Tukey's multiple comparison, error bars represent mean and SEM, * $P < 0.05$, ** $P < 0.01$. Uncropped western blots for showing *PSEN1* and Actin for each induction are provided in [Supplementary Fig. 2](#)

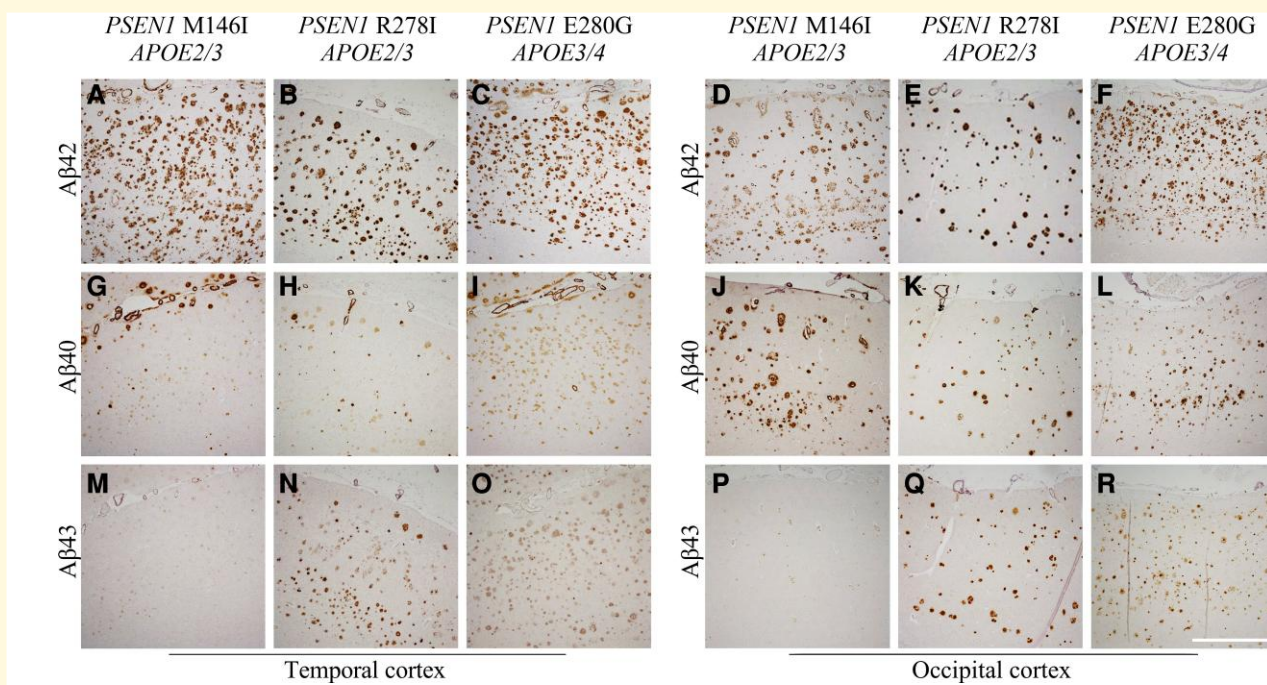


Figure 5 Cortical A β peptide deposition. Representative images of IHC performed on temporal cortex using antibodies specific to A β 42 (A–F), A β 40 (G–L) and A β 43 (M–R). White scale bar representing 100 μ m applies to all images

M146I line ($P=0.0008$), E280G.A line ($P=0.002$) and E280G.B line ($P=0.002$), see Fig. 4D.

qPCR data revealed no significant difference in the expression levels of PSEN1 across the control lines (pooled data), and the four FAD patient-derived lines (Fig. 4E). Together, these findings suggest that the PSEN1 E280G results in an accumulation of full-length PSEN1, *i.e.* the form that exists prior to autoproteolysis and maturation of PSEN1 protein fragments. However, unlike the R278I mutation that shows concurrently reduced levels of PSEN1-NTF, the data suggest no such effect of the E280G mutation.

A β peptide deposition in human post-mortem brain tissue

Post-mortem cortical brain tissue from three individuals with FAD carrying the same PSEN1 mutations that were studied in our cell lines (M146I, R278I and E280G) were available for immunohistochemical investigation. Note, the tissue and iPSC lines are not from the same individuals. The percentage area of A β -specific antibody coverage was assessed in the temporal and occipital cortices.

Immunohistochemical analysis displayed intense A β 42 deposition in all cases in the temporal (Fig. 5A–C) and occipital cortices (Fig. 5D and F). A β 42 was lowest in comparative regions in the R278I case (8.85 and 3.69%) compared with M146I and E280G mutations. In the temporal cortex the M146I and E280G cases had similar coverage (16.20 and 15.15%, respectively) while the M146I had lower coverage in the Occipital cortex (6.53%) compared to the E280G case (12.70%).

A β 40 pathology was present in all cases, notably as CAA, and cortical deposition (Fig. 5G–L). A β 40 was lowest in the R278I case (2.01 and 2.52%). In the temporal cortex, the E280G case had greater coverage (7.89%) compared to the M146I case (3.12%), however, this was reversed in the occipital cortex with greater coverage in the M146I case (6.04%) compared with the E280G case (3.86%).

A β 43 IHC shows mutation-specific differences in A β 43 deposition (Fig. 5G–R). A β 43 deposits can be observed as CAA and the prominent core of cored plaques, with varying intensity of cortical deposition and plaque type within and between cases. The lowest A β 43 was observed in the M146I case (0.09 and 0.14%), with greater coverage in the R278I (4.62 and 3.70%) and E280G cases (2.92 and 4.91%). These findings mirror the results for high A β 43 levels in conditioned media in the R278I and E280G cell lines.

Discussion

The pathogenic effect of mutations in PSEN1 is mediated through alterations in APP processing with different mutations producing distinct effects on that processing. This may potentially underlie some of the clinical heterogeneity seen in FAD mutation carriers. Here, for the first time, we have defined the consequences of the PSEN1 E280G mutation, which is associated with atypical clinical (spastic paraparesis) and pathological features (amyloid plaques of the cotton wool type). We have shown that in patient-derived iPSC-cortical neurons, the E280G mutation leads to increased ratios of A β 42 and of A β 43 compared with other

length peptides, which is linked with both reduced PSEN1 autoendoproteolysis and relative abundance of both full-length and PSEN1-NTF.

One way in which mutations can affect PSEN1 is via the initial endopeptidase activity of γ -secretase.^{42,43} Mutations which effect the endopeptidase activity could affect both absolute A β levels, and which pathway of A β production is selected, leading to altered ratios of the peptides within those pathways.²² Whilst *PSEN1* mutations vary in whether or not they alter the endopeptidase activity of γ -secretase, they have been found to consistently decrease the efficiency of its subsequent carboxypeptidase activity by destabilizing enzyme–substrate complexes between γ -secretase and the A β peptides it is processing.⁴⁴ The destabilization and compromised carboxypeptidase activity results in the release of longer A β peptides which are more prone to aggregation^{6,15,22} This in turn leads to more oligomeric A β and greater extracellular deposition.²³ We observed a greater A β 42:38 ratio in the M146I and E280G.A lines, compared with controls, indicative of consistently impaired carboxypeptidase activity in the A β 48 pathway for these lines. Mutations near the autoendoproteolysis site are proposed to inhibit the cleavage that converts the full-length form into the mature, cleaved product.²⁶ This can then lead to altered processivity by the enzyme.²⁷ Interestingly, even within the full-length PSEN1, the catalytic pore is still able to be formed,²⁸ which suggests that γ -secretase activity can still occur, although it is likely reduced, possibly explaining altered A β peptide production in mutations near this location. Such mutations in this region include PSEN1 R278I and E280G. Compared with controls and with M146I, the R278I and E280G lines displayed an increased A β 43:40 ratio, indicating reduced carboxypeptidase activity in the A β 49 pathway in a mutation dependant manner. Mutations not within the catalytic domain can likely affect the protein structure/stability and this may also impact interactions with substrates which will contribute to disease.^{20,24,41,44} For instance, the M146I mutation is not within the catalytic domains, yet displayed altered A β production profiles compared with controls, and other mutations.

Western blot analysis revealed a significantly increased full-length PSEN1 in the *PSEN1* R278I cell line compared with the control group. This has previously been shown for the R278I line, with a significant increase in full-length PSEN1 observed, and has been linked to A β 43 production.^{17,19,29,30} It has also been observed for the E280G mutation,²⁰ with our results suggestive of a trend for increased full-length PSEN1 in the E280G cell lines, although this did not reach significance.

The levels of PSEN1-NTF protein were also observed to be higher, and significantly so in the E280G neurons. As PSEN1 expression was not higher in these lines, it suggests that in the E280G lines there is an accumulation of PSEN1-NTF. This increase in PSEN1-NTF may explain the high levels of A β 42 observed in these lines, in addition to the high A β 43.

Finally, the level of full-length relative to PSEN1-NTF was significantly higher in the R278I line, which reflects the increase in products of the A β 49 pathway only in this line. This measure also highlights that the R278I mutation

specifically affects the processing of full-length to cleaved PSEN1, compared with other lines.

Similar to reported findings for the R278I mutation, the data presented in this study supports a similar effect of the E280G mutation, whereby PSEN1 protein maturation is affected. This is closely linked to the relative increase in A β 43 production. The findings by western blot corroborate with the results from the ELISA analysis, where high levels of A β 43 were observed in the *PSEN1* R278I and E280G mutation lines. It is likely that the mutation location hinders the processivity of full-length to cleaved PSEN1. The R278I and E280G mutations have a similar impact on A β ratios, however, the differential impacts on protein maturity effect may impact the amounts of mutant PSEN1 that are incorporated into the γ -secretase complex. Thus, absolute levels of A β could differ. To investigate this, isogenic lines with the homozygous mutations can be generated, as has previously been done for the PSEN1 Intron 4 deletion mutation.⁴⁵ This would allow the impact of these mutations to be assessed on protein maturity, A β ratios, and absolute A β levels, in the absence of a WT PSEN1 allele. It should be noted there was some variability between the two E280G lines. We cannot rule out that this could be due to the karyotypic abnormality in the E280G.A line in the 17q region. Although we were not able to identify the exact region that is duplicated, it is worth noting that the *MAPT* gene is located on chromosome 17q, encoding for tau, which forms pathological deposits in multiple dementias including FAD. Reassuringly, analysis of gene expression profiles in this line was normal (Supplementary Fig. 1) suggesting a minimal effect of this abnormality on stem cell health.

The mutation-associated differences in PSEN1 and subsequent A β production identified in this study are of particular interest in view of the distinct clinical and pathological features associated with the mutations we studied. E280G and R278I mutations both lie within exon 8, near the endoproteolytic cleavage domain. Mutations that are post-codon 200, and particularly within exon 8, have been linked to clinically atypical cognitive presentations and associated with spastic paraparesis.³² Motor symptoms have also been shown to be more frequent in *PSEN1* post-codon 200 cases.⁴⁶ Additionally, there are observed differences in age at onset related to *PSEN1* mutation location, with mutations beyond Codon 200 typically associated with a slightly later age at onset.^{32,47–49} Mutations beyond Codon 200 have also been found to show histological differences, with more severe amyloid deposition in the vasculature as CAA compared with mutations before Codon 200.⁴⁹ The study by Mann *et al.*⁴⁹ also found that the amount of cortical deposition of A β 42 correlated with cell line production of A β 42 in matched mutation cell line/tissue comparisons. While our case numbers were small, our histological observations support mutation-associated A β histological profiles and the A β specific IHC in matched mutation human cortical tissue corroborated our immunoassay findings. Both *PSEN1* R278I and E280G mutation cases displayed greater A β 43 deposition, while M146I did not, supporting mutation-specific alterations

in the A β 49 pathway. Interestingly, a recent report demonstrated that the *PSEN1* L435F mutation also leads to increased A β 43 in iPSC and post-mortem tissue, and thus our work expands the range of mutations known to specifically impact this peptide.⁵⁰ A β 40 deposition was apparent in all cases, which may be unexpected in the M146I case, as the immunoassays indicate alterations primarily in the A β 48 pathway. However, A β 40 is the most abundant A β peptide observed in human CSF including in Alzheimer's disease patients,^{51,52} and in human cell lines^{53,54} so some deposition could well be expected. Additionally, this case displayed A β 40 primarily as CAA, a predominant component of CAA.^{49,55,56} The M146I case has an apolipoprotein (*APOE*) ϵ 2/ ϵ 3 genotype. Generally, the *APOE* ϵ 4 allele is linked to sporadic CAA, with a meta-analysis indicating *APOE* ϵ 4 as a risk variant in grouped dementia patients and controls while *APOE* ϵ 2 may result in less CAA,^{57,58} although a positive *APOE* ϵ 4 carrier status and CAA severity were not associated in a study of *PSEN1* mutation cases.⁵⁹ Post-mortem analysis in 93 sAD patients revealed a significant association of CAA pathology with the *APOE* ϵ 4 allele, with increasing *APOE* ϵ 4 allele number associated with increasing severity of CAA.⁶⁰ However, the role of the *APOE* genotype in CAA is not clear cut, as carriers of the *APOE* ϵ 2 allele have been found to have more severe CAA than those with the *APOE* ϵ 3/ ϵ 3 genotype, despite the *APOE* ϵ 2 allele conferring lower risk for Alzheimer's disease.⁶¹ Additionally, Alzheimer's disease patients who were *APOE*2 carriers had worse small vessel disease⁶² and a meta-analysis found *APOE* ϵ 2 to be associated with certain markers of cerebrovascular disease.⁶³ These factors may contribute to the association between *APOE* ϵ 2 and CAA. Thus, the *APOE* ϵ 2 carriership in the M16I mutation case may influence the A β 40 pathology displayed in this case. However, the R278I case also has an *APOE* ϵ 2/ ϵ 3 genotype, which could also impact the histological observations. In future work, it would be of interest to investigate the A β peptides deposited in a larger number of individuals carrying the same FAD mutation but different *APOE* genotypes. Such larger studies will be needed in order to fully investigate correlations between clinical and pathological features and mutation-associated differences in A β processing. While studying pathology and iPSCs from the same individuals would be a gold standard, the altered A β ratios observed in iPSC studies are conserved in FAD and also in sAD human tissue, validating the use of iPSCs as models and implying γ -secretase alterations do occur *in vivo* and can occur in sAD.⁶⁴ Furthermore, the approach used here has enabled some confirmation of cell line results to human pathological tissue, highlighting the validity of the models to recapitulate FAD mechanisms and their appropriateness to investigate clinical and pathological associations.

Acknowledgements

The graphical abstract was created with BioRender.com. We would like to thank NanoString for early access to their stem

cell panel, as well as Xavier Tait and Bryan Serrels for technical advice and help with data analysis.

Funding

This work was supported by Alzheimer's Research UK (ARUKSRF-2016B-2, ARUKSRFEXT2020, ARUKSRFEXT2019B-001, ARUK-PhD2016-19). C.A. is supported by a fellowship from the Alzheimer's Society (AS-JF-18-008). H.Z. is a Wallenberg Scholar supported by grants from the Swedish Research Council (#2018-02532), the European Research Council (#681712), Swedish State Support for Clinical Research (#ALFGBG-720931), the Alzheimer Drug Discovery Foundation (ADDF), USA (#201809-2016862), the Alzheimer's Disease Strategic Fund and the Alzheimer's Association (#ADSF-21-831376-C, #ADSF-21-831381-C and #ADSF-21-831377-C), the Olav Thon Foundation, the Erling-Persson Family Foundation, Stiftelsen för Gamla Tjänarinnor, Hjärnfonden, Sweden (#FO2019-0228), the European Union's Horizon 2020 research and innovation programme under the Marie Skłodowska-Curie grant agreement No 860197 (MIRIAD), and the Medical Research Council UK Dementia Research Institute at University College London. N.S.R. is supported by a University of London Chadburn Academic Clinical Lectureship. The Queen Square Brain Bank is supported by the Reta Lila Weston Institute for Neurological Studies and the Medical Research Council. This work was supported by the National Institute for Health and Care Research University College London Hospital/University College London Biomedical Research Centre, the Rosetrees Trust, the Medical Research Council Dementia Platform UK and the UK Dementia Research Institute at University College London, which receives its funding from UK Dementia Research Institute Ltd, funded by the Medical Research Council, Alzheimer's Society and Alzheimer's Research UK.

Competing interests

H.Z. has served at scientific advisory boards for Alector, Eisai, Denali, Roche Diagnostics, Wave, Samumed, Siemens Healthineers, Pinteon Therapeutics, Nervgen, AZTherapies and CogRx; has given lectures in symposia sponsored by Cellectricon, Fujirebio, Alzecure and Biogen; and is a co-founder of Brain Biomarker Solutions in Gothenburg AB (BBS), which is a part of the GU Ventures Incubator Programme (all outside submitted work). N.C.F. has served on scientific advisory boards for Biogen and Roche and on a data safety monitoring board for Biogen; and has also provided consultancy to Ionis and Eli Lilly.

Supplementary material

Supplementary material is available at *Brain Communications* online.

Data availability

The authors confirm that all data supporting the findings of this study are available within the article and readily available upon request. Uncropped western blots for the data provided in Fig. 4 are provided in Supplementary Fig. 2.

References

- Braak H, Braak E. Neuropathological staging of Alzheimer-related changes. *Acta Neuropathol.* 1991;82(4):239-259.
- Thal DR, Rüb U, Orantes M, Braak H. Phases of β -deposition in the human brain and its relevance for the development of AD. *Neurology.* 2002;58(12):1791-1800.
- Hyman BT, Phelps CH, Beach TG, et al. National institute on aging-Alzheimer's association guidelines for the neuropathologic assessment of Alzheimer's disease. *Alzheimers Dement.* 2012;8(1):1-13.
- Goate A, Chartier-Harlin MC, Mullan M, et al. Segregation of a missense mutation in the amyloid precursor protein gene with familial Alzheimer's disease. *Nature.* 1991;349(6311):704-706.
- Sherrington R, Froelich S, Sorbi S, et al. Alzheimer's disease associated with mutations in presenilin 2 is rare and variably penetrant. *Hum Mol Genet.* 1996. 5(7):985-988.
- Scheuner D, Eckman C, Jensen M, et al. Secreted amyloid beta-protein similar to that in the senile plaques of Alzheimer's disease is increased in vivo by the presenilin 1 and 2 and APP mutations linked to familial Alzheimer's disease. *Nat Med.* 1996;2:864-870.
- Rovelet-Lecrux A, Hannequin D, Raux G, et al. APP Locus duplication causes autosomal dominant early-onset Alzheimer disease with cerebral amyloid angiopathy. *Nat Genet.* 2006;38(1):24-26.
- Kasuga K, Shimohata T, Nishimura A, et al. Identification of independent APP locus duplication in Japanese patients with early-onset Alzheimer disease. *J Neurol Neurosurg Psychiatry.* 2009;80(9):1050-1052.
- Sleegers K, Brouwers N, Gijselink I, et al. APP Duplication is sufficient to cause early onset Alzheimer's dementia with cerebral amyloid angiopathy. *Brain.* 2006;129(11):2977-2983.
- De Strooper B, Saftig P, Craessaerts K, et al. Deficiency of presenilin-1 inhibits the Normal cleavage of amyloid precursor protein. *Nature.* 1998;391(6665):387-390.
- Wolfé MS, Xia W, Ostaszewski BL, et al. Two transmembrane aspartates in presenilin-1 required for presenilin endoproteolysis and γ -secretase activity. *Nature.* 1999;398(6727):513-517.
- Vassar R, Bennett BD, Babu-Khan S, et al. β -Secretase cleavage of Alzheimer's amyloid precursor protein by the transmembrane aspartic protease BACE. *Science.* 1999;286(5440):735-741.
- Qi-Takahara Y, Morishima-Kawashima M, Tanimura Y, et al. Longer forms of amyloid β protein: Implications for the mechanism of intramembrane cleavage by γ -secretase. *J Neurosci.* 2005;25(2):436-445.
- Takami M, Sano Y, Ishihara S, et al. γ -Secretase: Successive tripeptide and tetrapeptide release from the transmembrane domain of β -carboxyl terminal fragment. *J Neurosci.* 2009. 29(41):13042-13052.
- Szaruga M, Veugelen S, Benurwar M, et al. Qualitative changes in human gamma-secretase underlie familial Alzheimer's disease. *J Exp Med.* 2015;212(12):2003-2013.
- Penney J, Ralvenius WT, Tsai L-H. Modeling Alzheimer's disease with iPSC-derived brain cells. *Mol Psychiatry.* 2019;25:148-167.
- Arber C, Toombs J, Lovejoy C, et al. Familial Alzheimer's disease patient-derived neurons reveal distinct mutation-specific effects on amyloid beta. *Mol Psychiatry.* 2019;25:2919-2931.
- Suárez-Calvet M, Belbin O, Pera M, et al. Autosomal-dominant Alzheimer's disease mutations at the same codon of amyloid precursor protein differentially alter β production. *J Neurochem.* 2014;128(2):330-339.
- Veugelen S, Saito T, Saido TC, Chávez-Gutiérrez L, De Strooper B. Familial Alzheimer's disease mutations in presenilin generate amyloidogenic β peptide seeds. *Neuron.* 2016;90(2):410-416.
- Sun L, Zhou R, Yang G, et al. Analysis of 138 pathogenic mutations in presenilin-1 on the in vitro production of A β 42 and A β 40 peptides by γ -secretase. *Proc Natl Acad Sci U S A.* 2017. 114(4):E476-E485.
- Murayama O., et al., *Enhancement of amyloid β 42 secretion by 28 different presenilin 1 mutations of familial Alzheimer's disease.* *Neurosci Lett.*, 1999. 265(1): p. 61-63.
- Chávez-Gutiérrez L, Bammens L, Benilova I, et al. The mechanism of γ -secretase dysfunction in familial Alzheimer disease. *EMBO J.* 2012;31(10):2261-2274.
- Selkoe DJ. Alzheimer's disease—genotypes, phenotype, and treatments. *Science.* 1997;275(5300):630-631.
- Bai X-C, Yan C, Yang G, et al. An atomic structure of human γ -secretase. *Nature.* 2015;525(7568):212-217.
- Thinakaran G, Borchelt DR, Lee MK, et al. Endoproteolysis of presenilin 1 and accumulation of processed derivatives in vivo. *Neuron.* 1996;17(1):181-190.
- Steiner H, Romig H, Pesold B, et al. Amyloidogenic function of the Alzheimer's disease-associated presenilin 1 in the absence of endoproteolysis. *Biochemistry.* 1999;38(44):14600-14605.
- Quintero-Monzon O, Martin MM, Fernandez MA, et al. Dissociation between the processivity and total activity of γ -secretase: Implications for the mechanism of Alzheimer's disease-causing presenilin mutations. *Biochemistry.* 2011;50(42):9023-9035.
- Takeo K, Watanabe N, Tomita T, Iwatsubo T. Contribution of the γ -secretase subunits to the formation of catalytic pore of presenilin 1 protein. *J Biol Chem.* 2012;287(31):25834-25843.
- Nakaya Y, Yamane T, Shiraiishi H, et al. Random mutagenesis of presenilin-1 identifies novel mutants exclusively generating long amyloid β -peptides. *J Biol Chem.* 2005;280(19):19070-19077.
- Saito T, Suemoto T, Brouwers N, et al. Potent amyloidogenicity and pathogenicity of β 243. *Nat Neurosci.* 2011;14(8):1023-1032.
- O'Riordan S, McMonagle P, Janssen JC, et al. Presenilin-1 mutation (E280G), spastic paraparesis, and cranial MRI white-matter abnormalities. *Neurology.* 2002. 59(7): p. 1108-1110.
- Ryan NS, Nicholas JM, Weston PSJ, et al. Clinical phenotype and genetic associations in autosomal dominant familial Alzheimer's disease: A case series. *Lancet Neurol.* 2016;15(13):1326-1335.
- Rogaeva E, Bergeron C, Sato C, et al. PS1 Alzheimer's disease family with spastic paraplegia: The search for a gene modifier. *Neurology.* 2003;61(7):1005-1007.
- Dumanchin C, Tournier I, Martin C, et al. Biological effects of four PSEN1 gene mutations causing Alzheimer disease with spastic paraparesis and cotton wool plaques. *Hum Mutat.* 2006;27(10):1063.
- Wray S, Self M, Lewis PA, et al. Creation of an open-access, mutation-defined fibroblast resource for neurological disease research. *PLoS One.* 2012;7(8):e43099.
- Okita K, Matsumura Y, Sato Y, et al. A more efficient method to generate integration-free human iPSCs. *Nat Methods.* 2011; 8(5):409-412.
- Shi Y, Kirwan P, Smith J, Robinson HPC, Livesey FJ. Human cerebral cortex development from pluripotent stem cells to functional excitatory synapses. *Nat Neurosci.* 2012;15(3):477-486.
- Bergström P, Agholme L, Nazir FH, et al. Amyloid precursor protein expression and processing are differentially regulated during cortical neuron differentiation. *Sci Rep.* 2016;6:29200-29200.
- Ellis RJ, Olichney JM, Thal LJ, et al. Cerebral amyloid angiopathy in the brains of patients with Alzheimer's disease: The CERAD experience, part XV. *Neurology.* 1996;46(6):1592-1596.
- Draper JS, Smith K, Gokhale P, et al. Recurrent gain of chromosomes 17q and 12 in cultured human embryonic stem cells. *Nat Biotechnol.* 2004;22(1):53-54.

41. Somavarapu AK, Kepp KP. Loss of stability and hydrophobicity of presenilin 1 mutations causing Alzheimer's disease. *J Neurochem.* 2016;137(1):101-111.
42. Capell A, Steiner H, Romig H, *et al.* Presenilin-1 differentially facilitates endoproteolysis of the β -amyloid precursor protein and notch. *Nat Cell Biol.* 2000;2(4):205-211.
43. Bentahir M, Nyabi Omar, Verhamme Jan, *et al.* Presenilin clinical mutations can affect γ -secretase activity by different mechanisms. *J Neurochem.* 2006;96(3):732-742.
44. Szaruga M, Munteanu B, Lismont S, *et al.* Alzheimer's-Causing mutations shift $a\beta$ length by destabilizing γ -secretase- $a\beta$ n interactions. *Cell.* 2017;170(3):443-456.e14.
45. Arber C, Villegas-Llerena C, Toombs J, *et al.* Amyloid precursor protein processing in human neurons with an allelic series of the PSEN1 intron 4 deletion mutation and total presenilin-1 knockout. *Brain Commun.* 2019;1:fcz024.
46. Vöglein J, Paumier K, Jucker M, *et al.* Clinical, pathophysiological and genetic features of motor symptoms in autosomal dominant Alzheimer's disease. *Brain.* 2019;142(5):1429-1440.
47. Lippa CF, Swearer JM, Kane KJ, *et al.* Familial Alzheimer's disease: Site of mutation influences clinical phenotype. *Ann Neurol.* 2000; 48(3):376-379.
48. Shea YF, Chu L-W, Chan AO-K, *et al.* A systematic review of familial Alzheimer's disease: Differences in presentation of clinical features among three mutated genes and potential ethnic differences. *J Formos Med Assoc.* 2016;115(2):67-75.
49. Mann DMA, Pickering-Brown SM, Takeuchi A, Iwatsubo T. Amyloid angiopathy and variability in amyloid β deposition is determined by mutation position in presenilin-1-linked Alzheimer's disease. *Am J Pathol.* 2001;158(6):2165-2175.
50. Oakley DH, Chung M, Klickstein N, Commins C, Hyman BT, Frosch MP. The Alzheimer disease-causing presenilin-1 L435F mutation causes increased production of soluble AB43 species in patient-derived iPSC-neurons, closely mimicking matched patient brain tissue. *J Neuropathol Exp Neurol.* 2020;79(6):592-604.
51. Fukuyama R, Mizuno T, Mizuno T, *et al.* Age-Dependent change in the levels of A β 40 and A β 42 in cerebrospinal fluid from control subjects, and a decrease in the ratio of A β 42 to A β 40 level in cerebrospinal fluid from Alzheimer's disease patients. *Eur Neurol.* 2000; 43(3):155-160.
52. Mehta PD, Pirttilä T, Mehta SP, *et al.* Plasma and cerebrospinal fluid levels of amyloid β proteins 1-40 and 1-42 in Alzheimer disease. *Arch Neurol.* 2000;57(1):100-105.
53. Asami-Odaka A, Ishibashi Y, Kikuchi T, Kitada C, Suzuki N. Long amyloid. β -protein secreted from wild-type human neuroblastoma IMR-32 cells. *Biochemistry.* 1995;34(32):10272-10278.
54. Turner RS, Suzuki N, Chyung ASC, Younkin SG, Lee VM-Y. Amyloids and are generated intracellularly in cultured human neurons and their secretion increases with maturation. *J Biol Chem.* 1996;271(15):8966-8970.
55. Iizuka T., *et al.*, Amyloid β -protein ending at Thr43 is a minor component of some diffuse plaques in the Alzheimer's disease brain, but is not found in cerebrovascular amyloid. *Brain Res.*, 1995. 702-(1-2): p. 275-278.
56. Savage MJ, Kawooya JK, Pinsky LR, *et al.* Elevated $a\beta$ levels in Alzheimer's disease brain are associated with selective accumulation of $a\beta$ 42 in parenchymal amyloid plaques and both $a\beta$ 40 and $a\beta$ 42 in cerebrovascular deposits. *Amyloid.* 1995;2(4):234-240.
57. Rannikmäe K, Samarasekera N, Martinez-Gonzalez NA, Al-Shahi Salman R, Sudlow CLM. Genetics of cerebral amyloid angiopathy: Systematic review and meta-analysis. *J Neurol. Neurosurg Psychiatry.* 2013;84(8):901-908.
58. Rannikmäe K, Kalaria RN, Greenberg SM, *et al.* APOE Associations with severe CAA-associated vasculopathic changes: Collaborative meta-analysis. *J Neurol Neurosurg Psychiatry.* 2014;85(3):300-305.
59. Mann DMA, Takeuchi A., Sato S, *et al.* Cases of Alzheimer's disease due to deletion of exon 9 of the presenilin-1 gene show an unusual but characteristic β -amyloid pathology known as 'cotton wool' plaques. *Neuropathol Appl Neurobiol.* 2001;27(3):189-196.
60. Sakae N, Heckman MG, Vargas ER, *et al.* Evaluation of associations of Alzheimer's disease risk variants that are highly expressed in microglia with neuropathological outcome measures. *J Alzheimer's Dis.* 2019;70(3):659-666.
61. Nelson PT, Pious NM, Jicha GA, *et al.* APOE- ϵ 2 and APOE ϵ 4 correlate with increased amyloid accumulation in cerebral vasculature. *J Neuropathol Exp Neurol.* 2013;72(7):708-715.
62. Groot C, Sudre CH, Barkhof F, *et al.* Clinical phenotype, atrophy, and small vessel disease in APOE2 carriers with Alzheimer disease. *Neurology.* 2018;91(20):E1851-E1859.
63. Schilling S, DeStefano AL, Sachdev PS, *et al.* APOE Genotype and MRI markers of cerebrovascular disease: Systematic review and meta-analysis. *Neurology.* 2013;81(3):292-300.
64. Sandebring A, Welander H, Winblad B, Graff C, Tjernberg LO. The pathogenic $a\beta$ 43 is enriched in familial and sporadic Alzheimer disease. *PLoS One.* 2013;8(2):e55847.